Supplementary Information:

Imaging magnetic spiral phases, skyrmion clusters, and skyrmion displacements at the surface of bulk Cu_2OSeO_3

Estefani Marchiori[1], Giulio Romagnoli[1], Lukas Schneider[1,2], Boris Gross[1], Pardis Sahafi[3,4], Andrew Jordan[3,4], Raffi Budakian[3,4], Priya R. Baral[5,6], Arnaud Magrez[6], Jonathan S. White[5] and Martino Poggio[1,2*]

[1]Department of Physics, University of Basel, 4056, Basel, Switzerland.
[2]Swiss Nanoscience Institute, University of Basel, 4056, Basel, Switzerland.
[3]Department of Physics and Astronomy, University of Waterloo, N2L 3G1, Waterloo, Canada.
[4]Institute for Quantum Computing, University of Waterloo, N2L 3G1, Waterloo, Canada.
[5]Laboratory for Neutron Scattering and Imaging, Paul Scherrer Institute, 5232, Villigen PSI, Switzerland.
[6]Institute of Physics, École Polytechnique Fédérale de Lausanne, 1015, Lausanne, Switzerland.

*Corresponding author(s). E-mail(s): martino.poggio@unibas.ch;

Supplementary Note 1:

Sample characterization

The crystal is a roughly rectangular cuboid with dimensions $2.4 \times 1.9 \times 1.1$ mm^3. After a natural {100} facet of the Cu_2OSeO_3 crystal is chosen as the surface for investigation, it is mechanically polished, and its orientation is verified via X-ray diffraction using the Laue method. As shown in Supp. Fig. 1(a), the pattern is consistent with a {100} surface. Supp. Fig. 1(b) shows the crystallographic directions and faces, which are identified based on the X-ray diffraction and measurements of the physical angles between natural faces.

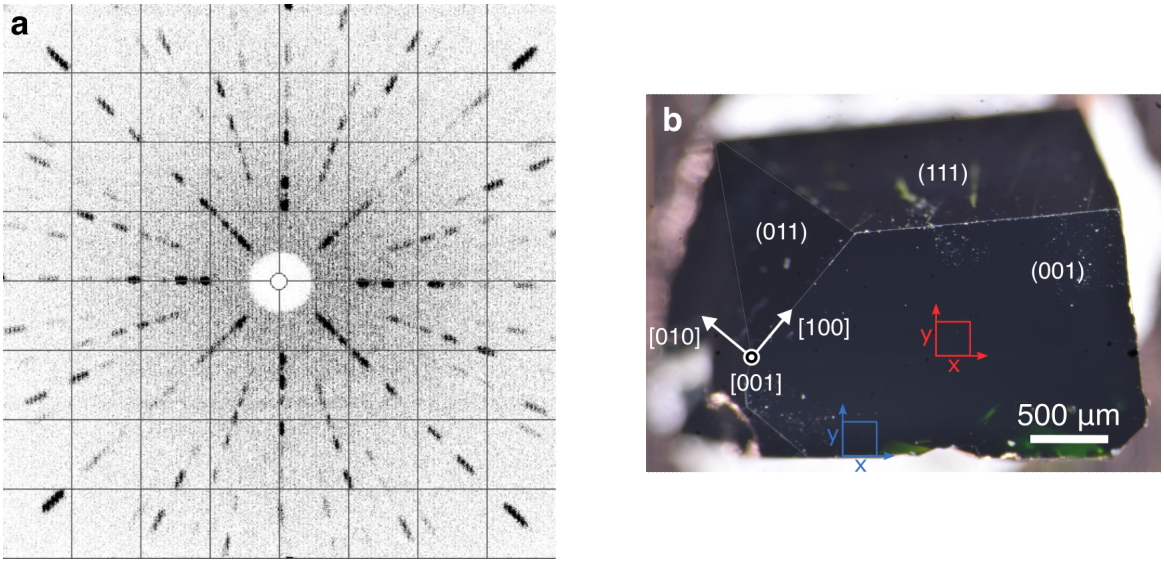

Supp. Fig. 1 Cu_2OSeO_3 crystallographic orientations. (a) Four-fold symmetric diffraction pattern obtained using X-ray Laue on the scanned (001) surface of the Cu_2OSeO_3 single crystal after mechanical polishing. (b) Optical micrograph of the crystal with labeled crystallographic axes and planes. The location of the SSM scanning window is represented in red, and the MFM scanning window is in blue, with both sizes exaggerated for clarity. The edges of the crystal have also been highlighted for clarity.

Before imaging by scanning SQUID microscopy (SSM), the (001) surface is etched using Ar plasma, and the resulting roughness is measured by atomic force microscopy (AFM). As shown in Supp. Fig. 2, the surface has a roughness of 5 nm with a lateral feature size of 70-130 nm.

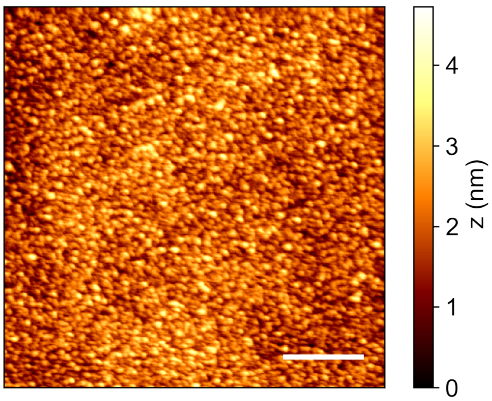

Supp. Fig. 2 Atomic force micrograph of the (001) surface of the same Cu_2OSeO_3 crystal measured and described in the main text. The image shows an approximate roughness of 5 nm on a characteristic length scale of 70-130 nm. Scalebar: 1 μm.

Supplementary Note 2:

Magnetic scanning probe microscopy techniques

Supp. Figs. 3(a) and (b) show schematic drawings of the nanowire-based magnetic force microscopy (MFM) and scanning SQUID microscopy (SSM) setups, respectively.

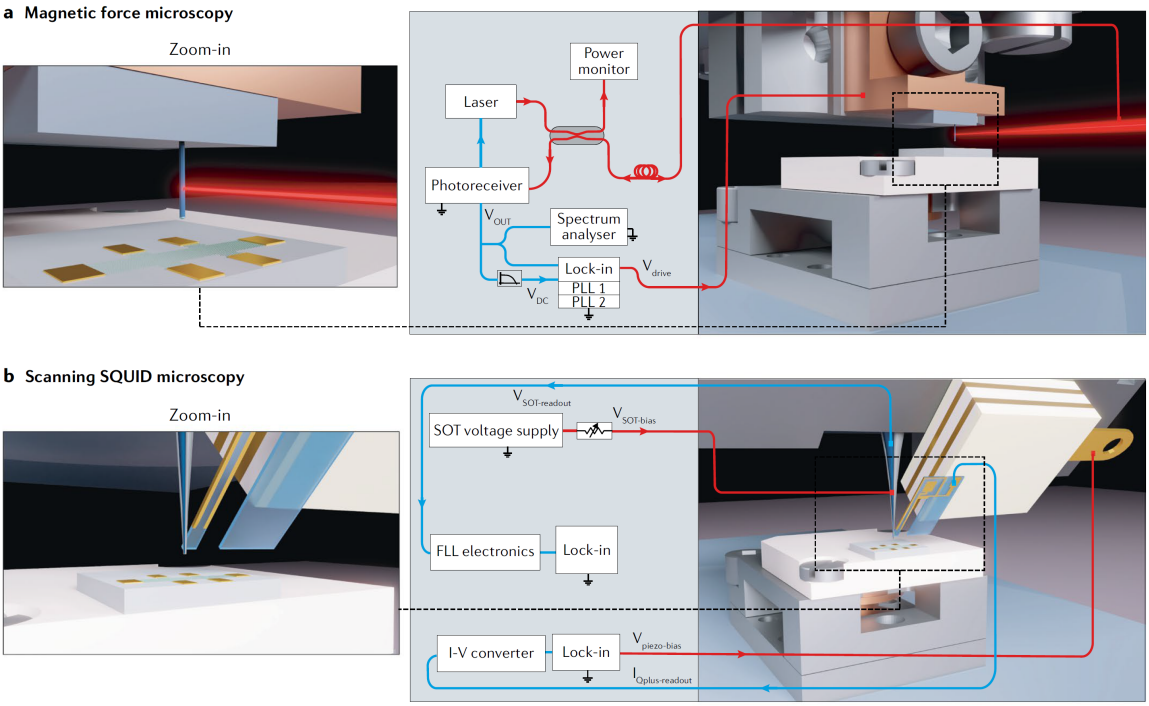

Supp. Fig. 3 Scanning probe microscopy apparatus. Each diagram shows a sample mounted on a movable stage, actuated by piezoelectric positioners. For scale, the white sample holder in each diagram is 12×12 mm in lateral size. Above this sample is the scanning probe, along with its corresponding readout scheme. Insets show zoomed-in views of each probe, which more clearly depict the detection schemes. (a) For nanowire magnetic force microscopy, focused laser light (red) is used for interferometric detection of the nanowire's flexural motion. (b) For scanning SQUID microscopy, a mechanically coupled tuning fork is used for tip–sample distance control. Figure adapted from Marchiori et al. [1]

Supplementary Note 3:

Additional scanning SQUID microscopy images

Supp. Fig. 4 shows maps of the stray magnetic field component perpendicular to the (001) surface, B_z, corresponding to the B_z^{ac} maps shown in Fig. 2 of the main text. This contrast is measured simultaneously to B_z^{ac} by the SQUID-on-tip probe. Although B_z gives a clearer picture of whether the underlying magnetization points along or against the applied field (bright points along $\hat{z}$ and dark points along $-\hat{z}$), it is noisier and has a lower spatial resolution than B_z^{ac}.

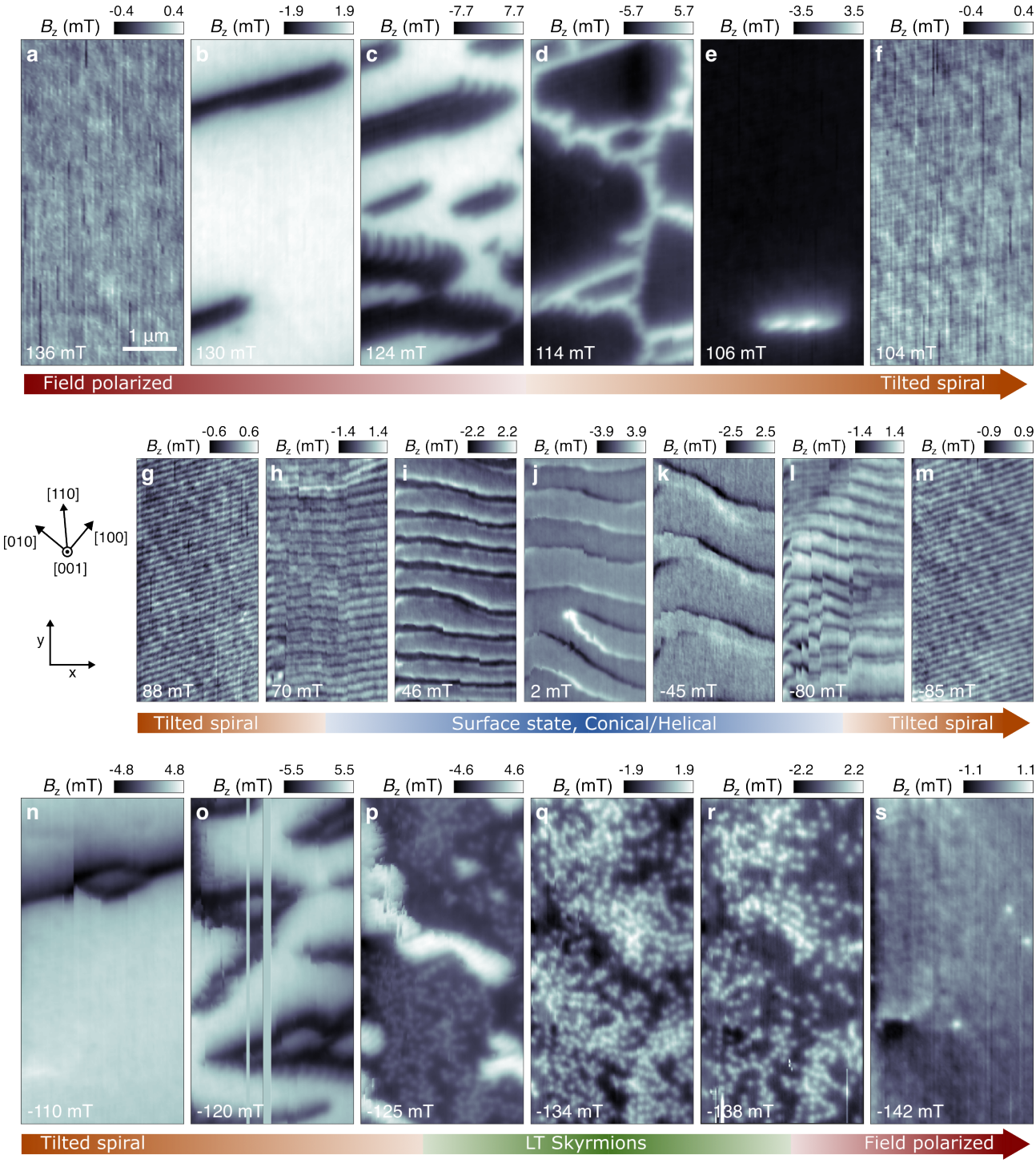

Supp. Fig. 4 SSM of magnetic phases at the surface of Cu_2OSeO_3. (a)-(s) Images of B_z at $T = 5$ K and in magnetic fields $\mu_0 H$ applied along [001], as indicated in the bottom left of each image.

Supplementary Note 4:

Small angle neutron scattering measurements

We carry out small angle neutron scattering (SANS) measurements on the same sample, which is measured by SSM and MFM, using the same temperature and field protocol. Supp. Figs. 5(a) and (c) correspond to measurements performed with the neutron beam perpendicular to the magnetic field applied along the [001] crystal direction, and Supp. Figs. 5(d)-(f) correspond to measurements performed with the neutron beam parallel to the applied magnetic field. Neutron scattering in the parallel configuration is only recorded in reverse field. SANS contrast confirms the presence of the helical, conical, tilted spiral, and low-temperature skyrmion phases. In the low-field range around zero, SANS measurements indicate the presence of helices along the three ⟨100⟩-type crystallographic directions, shown in Supp. Figs. 5(b) and (e), both in zero field. SANS measurements shown in Supp. Figs. 5(a) and (c) confirm that, in this sample, the temperature and field protocol used in the measurements described in the main text results in a significantly higher density of skyrmions in reverse applied field compared to forward applied field. This hysteresis likely explains the absence of skyrmions in SSM images of the surface taken in forward applied field and their presence in reverse applied field (see Supp. Fig. 4 or Fig. 2).

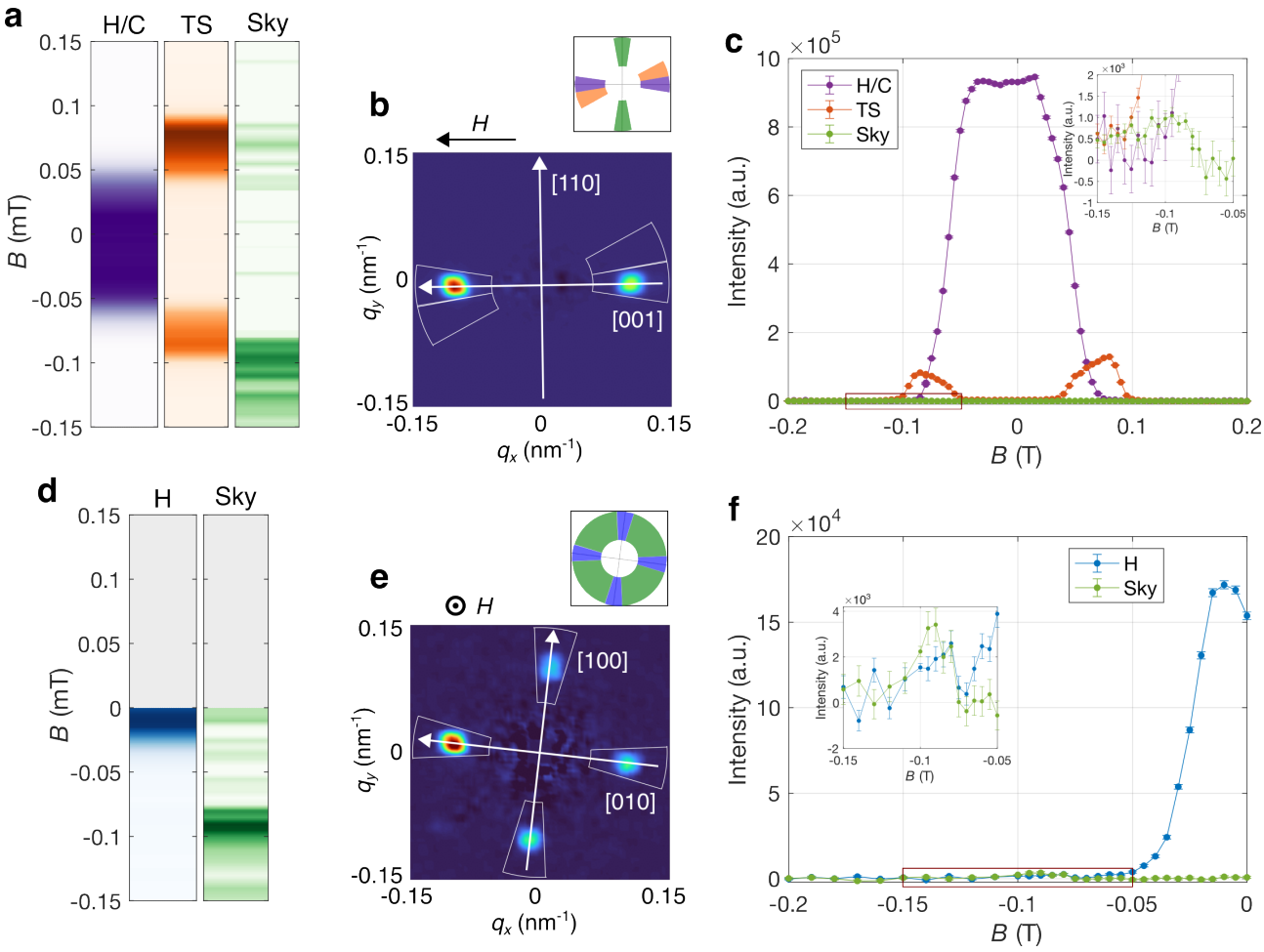

Supp. Fig. 5 Small angle neutron scattering (SANS) of Cu_2OSeO_3 crystal investigated by SSM and MFM. (a) Scattering intensities as a function of applied magnetic field with neutron beam perpendicular to magnetic field for window ranges shown in (b). Color scales have been rescaled to the maxima of each type of contrast. (b) Corresponding scattering plane in zero field. (c) Scattering intensities as a function of applied magnetic field for selected window ranges. (d) Scattering intensities as a function of applied magnetic field with neutron beam parallel to the applied magnetic field for window ranges shown in (e). Color scales have been rescaled to the maxima of each type of contrast. (e) Corresponding scattering plane in zero field. (f) Scattering intensities as a function of applied magnetic field for selected window ranges.

Supplementary Note 5:

Simulations of skyrmion pair distribution functions

In order to aid the interpretation of our measured skyrmion pair distribution, we simulate a regular skyrmion lattice of 70 nm spacing with an increasing degree of disorder. In particular, we simulate a regular skyrmion lattice with a diluted and random skyrmion site filling. Supp. Fig. 6(a) shows the locations of randomly distributed skyrmions in a perfectly regular lattice with a similar density as our experimental data, along with its corresponding 2D histogram of the pair distribution function $G_p(\mathbf{r})$. We consider the effect of a random deviation in the skyrmion position of 10% and 20% from a regular lattice, as shown in Supp. Figs. 6(b) and (c), respectively. Above 20% deviation, the signatures of translational or orientational order in $G_p(\mathbf{r})$ are lost, as in the $G_p(\mathbf{r})$ measured at the surface of Cu_2OSeO_3.

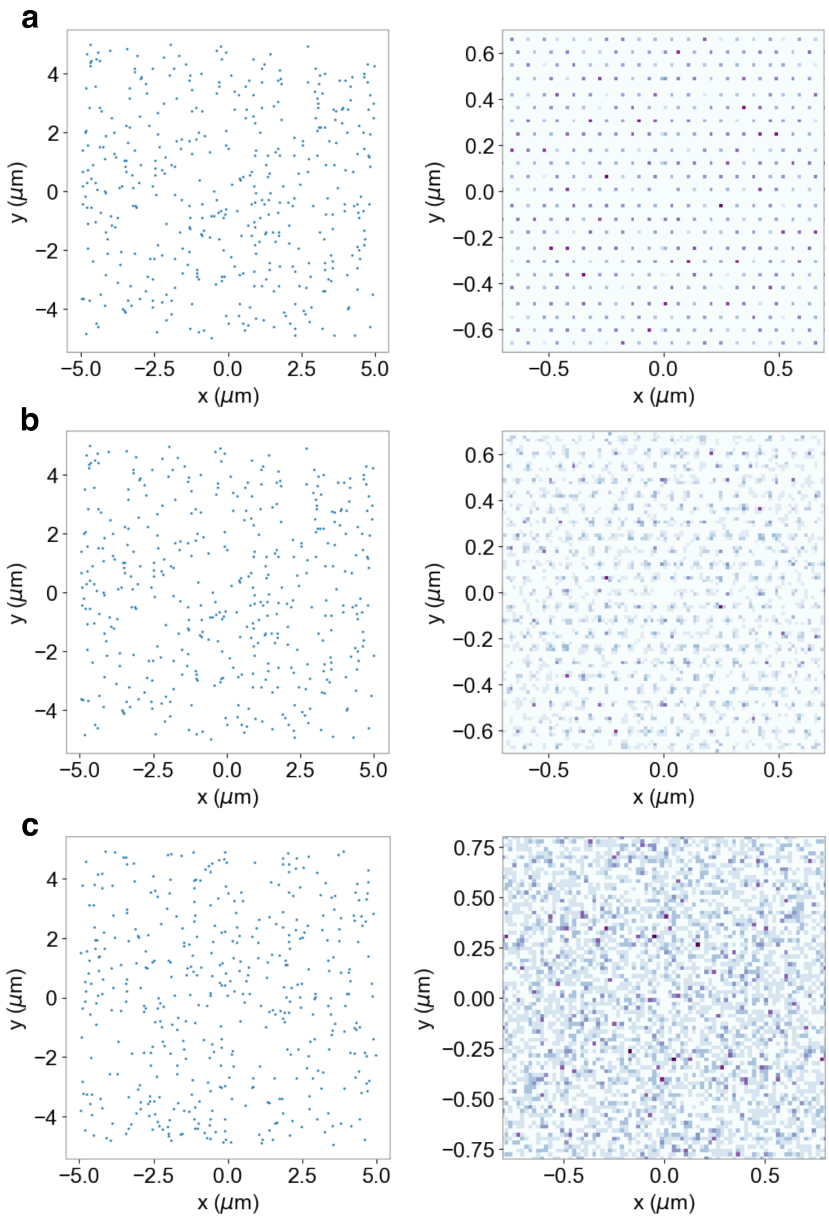

Supp. Fig. 6 Skyrmion lattice simulations with varying degrees of disorder. Each row shows the location of skyrmions in a lattice and the corresponding pair distribution function $G_p(\mathbf{r})$, (a) with a low skyrmion filling number and perfect lattice periodicity, (b) with a low skyrmion filling number and 10% random deviation from perfect periodicity, and (c) with a low skyrmion filling number and 20% random deviation from perfect periodicity.

Supplementary Note 6:

Spatial resolution of scanning SQUID microscopy

As discussed in the 'Scanning SQUID microscopy' section of the 'Methods', we use scanning SQUID-on-tip sensors with effective diameters of 80 and 110 nm, as measured by the periodicity of the critical current as a function of applied magnetic field. Although we do not have access to the precise transfer function of each probe, these diameters provide rough estimates for the full width at half maximum (FWHM) of their transfer functions. As a result, we can estimate the best-case spatial resolution.

A common way to define the spatial resolution of an imaging technique is the smallest distance between two point-like objects, for which each appears distinct. For example, if we take a probe approximated by a Gaussian tip transfer function with a FWHM of 100 nm ($\sigma = 0.43 \cdot \mathrm{FWHM} = 43$ nm) that is scanned much closer than its FWHM to the surface, it will image point-like objects (delta-function field profiles) as a convolution of the tip transfer function with the point-like objects. Each will simply appear as an image of the Gaussian tip transfer function. Two such Gaussians can be distinguished down to a separation of 2σ. This is the separation, below which the minimum between the two nearby Gaussians disappears (Sparrow criterion). For a 100-nm-diameter tip, this gives a spatial resolution of 86 nm.

Resolving two skyrmions in our SSM images is a more complex question. The smallest inter-skyrmion distance for which two skyrmions appear distinct is affected not only by the tip transfer function, but also by the size of the skyrmions themselves, which do not have a delta-function field profile, the tip-sample distance, which is between 80 and 100 nm, and the measurement noise. As can be seen in Supp. Fig. 7, by looking at the measurement itself, i.e. line-cuts of the closest pairs of nearby skyrmion dips that are still distinguishable, we can state that the SSM probe, which has an effective diameter of 110 nm and is used in Supp. Fig. 7, resolves skyrmions down to distances of at least 105 nm. This resolution is consistent with Gaussian fits to the individual skyrmion field profiles, which yield $2\sigma = 95$ nm, i.e. just below this experimentally determined resolution.

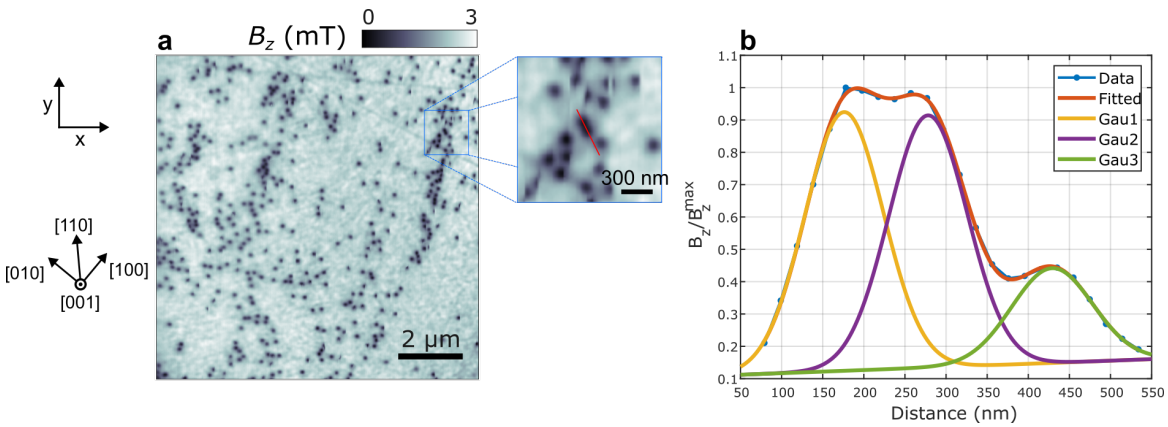

Supp. Fig. 7 Spatial resolution. (a), B_z image of skyrmions, as in Fig. 7, showing clusters of skyrmions with a zoomed in view showing the field profiles of three nearby skyrmions. (b) Linecut along the red line in (a) with the measurement shown as points, while Gaussian fits to each skyrmion profile and the sum of these profiles are shown as lines color-coded according to the legend. The linecut goes through the middle of the two skyrmions on the left of the plot, cutting the profiles through the center. The linecut does not go through the center of the third skyrmion on the right, resulting in a Gaussian fit with smaller amplitude and larger width than the others. Gaussian fits to the skyrmion pair on the left yield $2\sigma = 95$ nm. The skyrmions still appear distinct in the total profile because of the dip in the center. The distance between the center of the two Gaussian peaks is 105 nm, which is just above 2σ and sets an experimentally determined spatial resolution.

Note that SSM probes like those used here, with a transfer function larger than the skyrmion diameter, cannot reveal details about the skyrmion's internal structure, because the image of its field profile is blurred by the convolution process. For this reason, we cannot draw any conclusions about the internal structure of the observed skyrmions.

Another related quantity is the smallest possible skyrmion displacement that we can measure by SSM, i.e. the precision with which we can determine the difference between the position of a skyrmion in one image and in a subsequent image. This depends on a number of factors, including how precisely the position of each skyrmion can be determined and how well consecutive images can be aligned. These factors, in turn, depend on parameters, including pixel size and the signal-to-noise ratio. From the consecutive images shown in Fig. 8, we can determine skyrmion displacements with a precision better than 10 nm. This error is dominated by the error incurred in lining up consecutive images that have slightly drifted apart from one scan to the next. We do this by offsetting one image until we optimally cancel the $\Delta B_z(x, y)$ contrast from the vast majority of skyrmions, whose positions have not changed. Although the pixel size in these images is 20 nm, interpolation and high signal-to-noise ratio allow us to achieve a sub-pixel precision in this alignment, as shown in Supp. Fig 8.

In the section 'Skyrmion manipulation', we report values for the average displacement of a group of skyrmions. These averages are reported with errors given by the standard deviation of the different measurements. This deviation is much larger than the precision of the displacement measurement mentioned above.

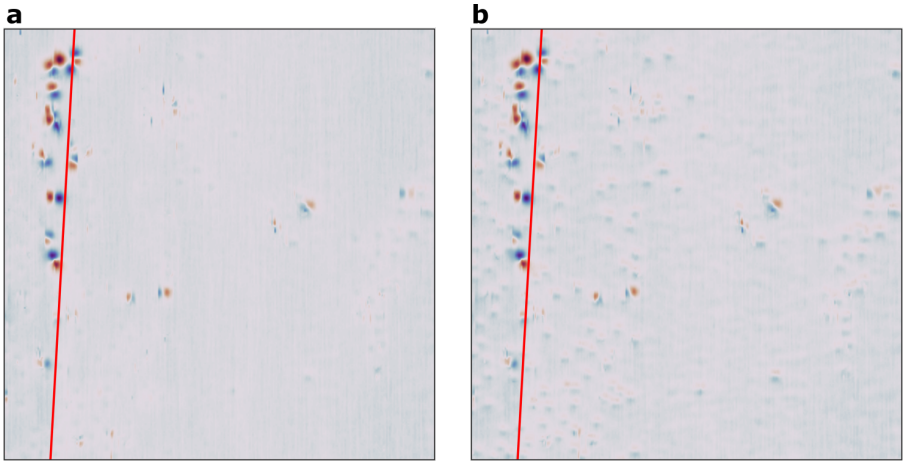

Supp. Fig. 8 Aligned and misaligned ΔB_z images. (a) ΔB_z image similar to those in Fig. 8 in which the B_z^{before} and B_z^{after} images have been aligned to compensate for drift by minimizing the contrast from the majority of features, whose positions do not change. (b) ΔB_z image showing a misalignment of B_z^{before} and B_z^{after} of 10 nm relative to the image in (a). The difference is clearly visible, allowing us to align the images with a precision better than 10 nm.

References

[1] Marchiori, E., Ceccarelli, L., Rossi, N., Lorenzelli, L., Degen, C.L., Poggio, M.: Nanoscale magnetic field imaging for 2D materials. Nature Reviews Physics **4**(1), 49–60 (2022). https://doi.org/10.1038/s42254-021-00380-9